Numerical Analysis of the Grasp Configuration of a planar 3-DOF Linkage-Driven Underactuated Finger

Hamed Khakpour
PhD student
Mechanical Engineering Department
Ecole Polytechnique of Montreal
Montreal, QC, CANADA, H3T 1J4
Email: hamed.khakpour@polymtl.ca

Lionel Birglen
Associate Professor, Member of ASME
Mechanical Engineering Department
Ecole Polytechnique of Montreal
Montreal, QC, CANADA, H3T 1J4
Email: lionel.birglen@polymtl.ca

ABSTRACT

This paper proposes a novel method to investigate the grasp sequence of an underactuated (a.k.a. adaptive) finger with three degrees of freedom but only one actuator and find its final configuration. This method considers the magnitude and the sign of the torques generated on the phalanges of the finger through the contact points. By using these torques as indices, the algorithm calculates the values of the joint angles during the grasping sequence until the finger reaches its final configuration. To illustrate the effectiveness of this method a class of a 3-DOF adaptive finger is chosen and analyzed and then using the proposed methodology, its grasp configuration is calculated when grasping different fixed objects. Finally, simulations are repeated using a dynamic simulation package and the obtained results are compared to the proposed method. The results show that the method can properly estimate the final configuration of the grasp.

Keywords: *grasp configuration, underactuated finger, self-motion, numerical method*

1 Introduction

So far, many different types of dexterous robotic hands have been designed and manufactured to grasp objects. However, these robotic hands usually have complicated mechanical structure, control system and operational performance. Thus, to

improve the simplicity of the control algorithm, decrease costs and achieve a more robust operating mode, many researches have been carried out on the field of underactuated, or adaptive, robotic hands [1–3].

Underactuated hands are a special type of end-effectors which are characterized by a larger number of degrees of freedom (DOFs) than actuators [4–6]. Although the number of actuators is reduced, they are still capable of adapting their contact areas to the shape of the grasped objects [3, 7]. Generally, underactuated mechanisms in robotic hands are classified in three broad categories namely, differential, compliant, and triggered mechanisms [8]. Although most underactuated hands belong to the first category, the others can also be employed, either concurrently with the first technique [5,9] or independently (e.g., fully compliant underactuated finger proposed in [10]).

Normally, two components are used in the structure of an underactuated hand, i.e., transmission system which distributes the actuation power among the driven joints, and passive elements (e.g., mechanical limits and springs) which sustain fingers initial configuration in the pre-grasp period and constrain its motion during the closing sequence (using these components is not mandatory and in some underactuated hands such as Soft Gripper [11] and Graspar [12], no spring is used). A typical closing sequence of an underactuated finger is illustrated in Fig. 1.

Regarding how the actuation power is transmitted, two main types of mechanisms are found: either tendon-driven or linkage-based mechanisms [2, 4, 7]. Tendon-actuated mechanisms may be the oldest type of underactuated fingers and their analysis is usually simpler than their linkage-based counterparts [4]. The Soft Gripper [11], SPRING hand [13], 100 G Hand [14], RTR2 Hand [15], and RL1 hand [16] are a few examples of tendon-driven underactuated fingers. When large grasping forces are required linkage-based mechanisms are usually preferred to the previous transmission system [17]. The MARS and SARAH prototypes [18, 19], IIM Robotic Hand [20], and AR hand III [21] are examples of these hands.

It should be made clear that despite being referred to as "underactuated" all these fingers are different from underactuated robots (in which the dynamics of the mechanisms is used to control their non-actuated axes) because, as a result of shape adaptive properties of underactuated fingers, their non-actuated axes can be constrained by either passive elements (if exist) or contacts with the grasped object. The most challenging issue in the field of underactuated hands hindering them in comparison with dexterous robotic hands is their ability to maintain a stable grasp. Stable grasp of a fixed object by a single underactuated finger is achieved if all phalanges with contact with the object have non-negative forces and the others with no contact have zero forces so that a static equilibrium is established [4]. For the stability of an underactuated hand, in addition to this condition for each finger, the form/force closure condition of the entire mechanism is also required to be able to grasp an object and completely constrain its motion while an external wrench exists [9]. With fully actuated hands, each phalanx of the finger can be controlled independent of the shape and location of the enveloped object, but with underactuated hand the stability of the finger depends on all these parameters. More specifically, the stability of these fingers is strongly related to the existence and the location of contact points.

Recently, particular efforts were made to study and analyze stable underactuated grasps. Kaneko et al. [22] introduced the notion of self-posture changeability of the fingers during the grasping of unknown objects and then found the position of contact point between the finger and the object (which is assumed to be fixed). Afterwards, Birglen et al. [4, 23] studied the reconfiguration and the stability of an underactuated finger during the grasping of unknown objects described by fixed points

in space. They analyzed the stability of 2-DOF underactuated fingers and establish how it reconfigures if it is not stable after an initial contact with an object. Additionally, they tried to determine the stability of 3-DOF fingers and revealed different conditions affecting these issues without reaching a general methodology to determine whether a finger will be stable or not [4]. Next, Ciocarlie and Allen [24] introduced a quasi-static analysis method to predict whether an underactuated finger can grasp any arbitrary object and reach a stable configuration or if the closing motion will lead to losing that object. But, their strategy did not find the final configuration of the finger.

In all cases, the final grasp configuration of underactuated fingers with three or more DOFs is not fully predictable unless a complete dynamic modeling is done and the associated partial differential equation (PDE) is solved. Thus, a method is proposed in this paper to evaluate this property and calculate the final configuration of a 3-DOF underactuated finger. This method focuses on the process of grasping a fixed object using a single underactuated finger. Thus, the form/force closure condition is not aimed and so the existence of static equilibrium and non-negative forces are the key points of seeking for the final grasp configuration. In this algorithm, the following assumptions are considered:

1. The contact points are supposed to be fixed and known,
2. Each phalanx can have only one contact point with the object,
3. The phalanges and the transmission links of the finger have negligible masses and inertias. Also, the velocities of these links during the closing motion are low so the finger does not lose any contact due to dynamic effects (this algorithm is developed for a finger in which passive components are employed and these components play a significant role in minimizing the dynamic effects on the closing motion of the finger),
4. Gravity and friction are neglected,
5. The magnitude of the actuation torque of the finger increases step-by-step.

Considering these assumptions, to detect the contacts between the finger and the object, instead of using dynamic models such as rigid body model and compliant model (e.g., spring and damper system) [25] where dynamic parameters (i.e., velocity, acceleration, stiffness, damping, etc.) are considered, a static analysis is used. This way, knowing the direct kinematic of the planar 3-phalanx system of the finger, if a contact point is on the left hand side of the finger (considering the situation shown in Fig. 2), then it has not reached that point. Otherwise, that contact point is one of the boundaries of the motion of the finger and if a phalanx reaches this point it cannot pass it (the object and the phalanges are assumed rigid) and based on a static analysis the corresponding contact force is obtained.

To execute this method, a novel architecture recently proposed in [26] and termed S-class 3-DOF underactuated finger is selected as an example. This is the first time that this new finger is analyzed.

In the next section, this finger will be introduced; in Section three, all the required force equations will be shown; in Section four, the reconfiguration of the finger after its first contact will be analyzed and the procedure to find its final configuration will be defined; in Section five, the developed numerical method will be used to calculate the final posture of the finger when enveloping different objects and finally, the results will be compared with the outputs of the ADAMS software which is used as a commercial dynamic simulation software (DSS).

2 The S-class Underactuated Finger

The schematic of a typical 3-DOF S-class underactuated finger is shown in Fig. 2. As it can be seen in this figure, the finger is constituted of six binary links, one of them being the ground. Three consecutive links define the phalanges of the finger and the two remaining form the transmission linkage.

The actuation torque driving the finger is applied to the mechanism through the joint o_4 and θ_a is the associated joint angle. Springs are installed in joints o_2 and o_3. These two passive elements constrain the two remaining DOF of the finger. Using mechanical limits the angles of the intermediate and distal phalanges, measured by namely θ_2 and θ_3 are limited to be within $[0,90]$ degrees while for the proximal phalange, θ_1 is assumed to stay in the range of $[0,180]$ degrees to allow the finger to grasp an object regardless of its location with respect to the palm.

3 Calculating the Forces and the Torques on the Phalanges

To calculate the grasp configuration of the finger, the relationship between the input actuation torque and the output forces and torques exerted to the phalanges must be obtained. As presented in [4], this relationship can be obtained by calculating two matrices. The first one is the Transmission matrix which is a function of the type of the transmission system (e.g., gears, linkages, tendons, etc.) used in the design of the finger and also its geometrical configuration. The second matrix is the Jacobian of the finger which relates the contact force on each phalanx to the torque generated at its base. In this work, it is assumed that there is no friction between the phalanges and the object. Disregarding friction between the phalanges and the object might appear strange and unrealistic. However, the aim of the simulations done in this paper is to assist in the design of a finger. Thus, one would want to design a finger that will be stable for any contact parameters. It is therefore logical to consider the worst case scenario, namely, zero friction. Friction resists the motion of the phalanges so it can slow down or stop them. Thus, it decreases the risk of losing the grasped object and considering its effect, the final configuration of the finger depends on the friction coefficient and it is difficult to find an exact final configuration. Hence, only terms which are related to the normal forces in the contact points are considered in the Jacobian matrix.

The positive directions of all the forces exerted from the phalanges to the object are illustrated in Fig. 2. The magnitudes of the contact forces and the torques exerted on the phalanges depend on the existence of contact in the upper phalanges (the phalanges which are closer to the fingertip). Consequently, these forces and torques can be expressed as:

$$\tau = \mathbf{T}^T \boldsymbol{t}, \tag{1}$$

$$\boldsymbol{f} = \mathbf{J}^{-T} \tau, \tag{2}$$

where $\mathbf{T}$ is the Transmission matrix, $\mathbf{J}$ is the Jacobian matrix, $\boldsymbol{t}$ is the vector of actuation torques, τ is the vector of the torques exerted at the base of the phalanges and finally, $\boldsymbol{f}$ is the vector of the forces generated by the latter via the contact points.

These vectors are defined as:

$$\mathbf{t} = \begin{bmatrix} \tau_a \\ \tau_2 \\ \tau_3 \end{bmatrix}, \quad \tau = \begin{bmatrix} \tau'_1 \\ \tau'_2 \\ \tau'_3 \end{bmatrix}, \quad \text{and} \quad \boldsymbol{f} = \begin{bmatrix} f_1 \\ f_2 \\ f_3 \end{bmatrix}. \tag{3}$$

where τ_a is the actuation torque driving the finger in joint o_4; τ_2 and τ_3 are the passive torques due to the springs located in joints o_2 and o_3 and defined as $\tau_2 = -K_2\Delta\theta_2$ and $\tau_3 = -K_3\Delta\theta_3$ where K_2 and K_3 are the corresponding stiffness coefficients. Also, τ'_i and f_i for $i = 1,2,3$ are respectively the output torque and corresponding contact force. All the elements of these vectors are shown in Fig. 2.

3.1 Calculating the Transmission Matrix

The Transmission matrix $\mathbf{T}$ relates the vector ω_a of angular velocities in the joints hosting either the actuator or a spring to the angular velocities of the phalanx joints, i.e.:

$$\omega_a = \mathbf{T}\dot{\theta} \Longleftrightarrow \begin{bmatrix} \dot{\theta}_a \\ \dot{\theta}_2 \\ \dot{\theta}_3 \end{bmatrix} = \begin{bmatrix} X_1 & X_2 & X_3 \\ 0 & 1 & 0 \\ 0 & 0 & 1 \end{bmatrix} \begin{bmatrix} \dot{\theta}_1 \\ \dot{\theta}_2 \\ \dot{\theta}_3 \end{bmatrix}. \tag{4}$$

To find the element X_i relating $\dot{\theta}_a$ to $\dot{\theta}_i$ by using the principle of virtual work, one has to virtually lock the other phalanges (i.e., $\dot{\theta}_j = 0$ for $i \neq j$). As a result, the finger can only rotate around the i^{th} joint and the entire finger behaves as a single-DOF linkage (namely a four-bar). These conceptual four-bar linkages obtained by locking each set of two of the three phalanges of the finger are illustrated in Figs. 3a-c. As was shown in [27], the equation relating the input and the output angular velocities of four-bar linkages (equal to X_i) is then:

$$X_i = \frac{\dot{\theta}_a}{\dot{\theta}_i} = \frac{-r_i}{D_i - r_i}, \tag{5}$$

where r_i for $i = 1,2,3$ is:

$$r_i = \frac{A_i C_i \sin(\lambda_i + \theta_a - \alpha_i) - A_i D_i \sin(\alpha_i)}{C_i \sin(\lambda_i + \theta_a) - A_i \sin(\alpha_i)}, \tag{6}$$

with the lengths A_i, C_i and D_i as illustrated in Figs. 3a-c.

3.2 Calculating the Phalanges Torques When All have Contacts with an Object

The relationships between the input torques (vector **t**) and the torques exerted to the base joints of the phalanges (vector τ) can be expressed as:

$$\tau'_1 = X_1 \tau_a, \tag{7a}$$

$$\tau'_2 = X_2 \tau_a - K_2 \Delta\theta_2, \tag{7b}$$

$$\tau'_3 = X_3 \tau_a - K_3 \Delta\theta_3. \tag{7c}$$

The transpose of the inverse Jacobian matrix **J** in Eqn. (2), is obtained [4] as:

$$\mathbf{J}^{-T} = \begin{bmatrix} \frac{1}{k_1} & -\frac{k_2+L_1c_2}{k_1k_2} & -\frac{L_1(-c_2k_3-c_2c_3L_2+k_2c_{23})}{k_1k_2k_3} \\ 0 & \frac{1}{k_2} & -\frac{k_3+L_2c_3}{k_2k_3} \\ 0 & 0 & \frac{1}{k_3} \end{bmatrix}, \tag{8}$$

where $c_2 = \cos(\theta_2)$, $c_3 = \cos(\theta_3)$, $c_{23} = \cos(\theta_2+\theta_3)$, L_i for $i = 1,2,3$ is the length of the i^{th} phalanx and k_i for $i = 1,2,3$ is the distance between the i^{th} contact point and the base joint of the i^{th} phalanx as illustrated in Fig. 2. In Eqn. (8), the coefficient $\frac{1}{k_i}$ in the i^{th} row of the matrix can be factorized and combining with Eqn. (2) one obtains:

$$\begin{bmatrix} f_1k_1 \\ f_2k_2 \\ f_3k_3 \end{bmatrix} = \begin{bmatrix} 1 & -\frac{k_2+L_1c_2}{k_2} & -\frac{L_1(-c_2k_3-c_2c_3L_2+k_2c_{23})}{k_2k_3} \\ 0 & 1 & -\frac{k_3+L_2c_3}{k_3} \\ 0 & 0 & 1 \end{bmatrix} \begin{bmatrix} \tau'_1 \\ \tau'_2 \\ \tau'_3 \end{bmatrix}. \tag{9}$$

The left-hand side of Eqn.(9) is the vector of torques produced by the contact forces on the phalanges of the finger when all of them are in contact with the grasped object. Eventually, one has:

$$\tau''_1 = \tau'_1 - \frac{k_2+L_1c_2}{k_2}\tau'_2 - \frac{L_1(-c_2k_3-c_2c_3L_2+k_2c_{23})}{k_2k_3}\tau'_3, \tag{10a}$$

$$\tau''_2 = \tau'_2 - \frac{k_3 + L_2 c_3}{k_3}\tau'_3, \tag{10b}$$

$$\tau''_3 = \tau'_3. \tag{10c}$$

An important phenomenon particular to underactuated finger is that these torques can become negative even when the actuation torque is positive. This phenomenon prevents a stable grasp to be achieved in all situations and should be minimized by design. It is however arguably unavoidable for all contact configurations [4] and thus, must be simulated to ascertain if the negative torques will lead to a stable grasp with less than three contact points or to an ejection of the object from the finger.

3.3 Obtaining the Expression of the Torques in the Case of Missing Contacts

In addition to the previous case, the expression of the torques should also be obtained when there is no contact between certain phalanges and the seized object. For a 3-DOF finger there are 8 possible scenarios listed in Table 1.

Among the cases presented in this table, case 1 is detailed in the previous section and case 8 can be readily dismissed because there is no contact with the object and thus, no grasp per se exists. Since contact location on the proximal phalanx does not appear in Eqns. (10a-c), they can actually also be used in cases 2, 5, 6 and 7. However, in cases 5, 6 and 7 additional alterations of these equations are required. In cases 5 and 6, there is no contact on the distal phalanx, therefore, this phalanx can continue its closing motion up to when it reaches either its rotational limit or its movement is stopped by the spring if the input torque on this phalanx is not strong enough to overcome its resistance. In both cases, the finger loses one of its degrees of freedom and two last phalanges can be seen as a rigid body as the last joint is not rotating. Resultantly, in Eqns. (10a-c), the term τ'_3 is equal to 0. In case 7, the proximal phalanx makes contact with the object and two other phalanges continue their closing motion up to the moment when they are stopped by internal forces. Then, all three phalanges can be seen as a rigid body and the finger loses two DOF and behaves as a simple gripper. Consequently, in Eqns. (10a-c), the values of both τ'_2 and τ'_3 are 0 as well.

In the two remaining cases, namely 3 and 4, no contact point on the intermediate phalanx exists. Similar to the previous cases, since the expression of the contact with the proximal phalanx does not appear in Eqns. (10a-c), this formulation of the torque magnitudes, can again be used. For the finger to be in static equilibrium in these two cases, the term τ''_2 in Eqn. (10b) must be zero. Thus, τ'_2 is found to be:

$$\tau'_2 = \frac{k_3 + L_2 c_3}{k_3}\tau'_3. \tag{11}$$

Next, by substituting Eqn. (11) in Eqn. (10a) one can find τ''_1 as:

$$\tau''_1 = \tau'_1 - \frac{k_3 + L_2 c_3 + L_1 c_{23}}{k_3} \tau'_3. \tag{12}$$

Finally, the expression of τ''_3 can be calculated using Eqn. (10c). Eventually, the expressions of the torques which must be exerted to the grasped object via the contact points to keep the system in a static equilibrium are found for all possible contact cases.

4 Estimating the Self-motion of the Finger

When the finger collides with an object, based on the location and magnitudes of the generated contact force, its configuration will change. In the following sequence, the finger may gain new contacts or lose previous ones and this motion will be continued up to the point when the finger either reaches static equilibrium or loses the object. In this section, this change of posture is analyzed.

Considering the assumptions presented in the introduction, the dynamic problem of the closing motion of the finger can be turned into sets of discretized motions of the finger between pairs of configurations with static equilibrium corresponding to the infinitesimal increase of the actuation torque. Since the increase in the actuation torque is small, the configurations in which the finger evolves are very close.

The basis of the numerical method proposed in this paper is that during the grasping sequence, the finger will be stable if the values of the torques τ''_i are positive when there a contact point exists and zero if there is no contact. Additionally, the finger will reconfigure in such a manner that changes in the values of the joint angles depend on the magnitude and direction of these torques. These values are considered as an index to alter the angles of the corresponding joints until the static equilibrium is attained at each step when increasing the actuation torque.

Using this method, the evolution of each phalanx is evaluated separately by knowing the amount of torque exerted to it. In this way, the rotational movement of the i^{th} phalanx around its base joint is considered and by neglecting the effect of friction, its equation of motion is obtained as:

$$I_i \ddot{\theta}_i + \zeta_i \dot{\theta}_i = \tau''_i, \tag{13}$$

where I_i is the inertia of the i^{th} phalanx and ζ_i is the damping coefficient. Next, by discretizing this motion into sets of displacements in time steps Δt, this equation is rewritten as:

$$I_i \frac{\frac{\theta_i^j - \theta_i^{j-1}}{\Delta t} - \frac{\theta_i^{j-1} - \theta_i^{j-2}}{\Delta t}}{\Delta t} + \zeta_i \frac{\theta_i^j - \theta_i^{j-1}}{\Delta t} = \tau''_i, \tag{14}$$

where θ_i^j is the angle of the i^{th} joint in the j^{th} step. By simplifying Eqn. (14), one obtains:

$$\theta_i^j = \frac{(2+\frac{\Delta t\zeta_i}{I_i})\theta_i^{j-1} - \theta_i^{j-2} + \frac{\Delta t^2}{I_i}\tau''_i}{1+\frac{\Delta t\zeta_i}{I_i}}. \tag{15}$$

In this method, the value of the angle θ_i is obtained iteratively. Thus, taking into account the aforementioned assumptions, the terms $\frac{\Delta t\zeta_i}{I_i}$ and $\frac{\Delta t^2}{I_i}$ are respectively approximated by constant coefficients h_i and w_i and consequently the variation of the angle θ_i is modeled by the following iterative equation:

$$\theta_i^j = \frac{(2+h_i)\theta_i^{j-1} - \theta_i^{j-2} + w_i\tau''_i}{1+h_i}. \tag{16}$$

To compute the value of τ''_i at each iteration, the appropriate contact case should be selected from Table 1 and then, its value is obtained using the relevant equations amongst Eqns. (10a-c) and (12).

A flow chart of the algorithm is illustrated in Fig. 4. As can be seen in this figure, the algorithm begins the closing motion of the finger by rotating the phalanx around the axis o_1 and gradually increases the actuation torque. During this step, it searches for the existence of a contact between the phalanges and the object. If a contact is found it determines the contact case. Next, the relevant reconfiguration subroutine is used. These subroutines are all based on a similar algorithm, namely:

1. Taking the previous values of the joint angles of the finger.
2. Finding the other angles of the transmission linkage and the position of the identified contact points.
3. Calculating the values of the torques τ''_i for $i = 1,2,3$ based on the current actuation torque τ_a and the selection of the adequate equations amongst Eqns. (10a-c) and (12).
4. Checking the magnitudes and signs of these torques. In this step, if the current geometric configuration of the finger corresponds to a static equilibrium, the magnitude of τ_a is increased by a small amount and the algorithm returns to step 2.
5. Obtaining new values of joint angles with Eqn. (16).
6. Investigating the existence of new contact point(s) with the remaining phalanges. If such a case arises or the phalanges reach their mechanical limits then the subroutine is stopped, otherwise it goes back to step 2.

The subroutines have two levels: in the upper level the value of the actuation torque is increased and in the lower level it tries to find the set of angles which satisfy the equilibrium condition corresponding to the current value of τ_a. This moment denotes when the value of angle θ_i calculated from Eqn. (16) does not change in two consecutive iterations. The final configuration of the finger is identified in each of the aforementioned subroutines as a situation when by increasing the value of actuation torque in the upper level, the amount of joint angles of the finger do not change anymore. During this process, if ejection occurs, the algorithm will find which contact is lost and proceed with the closing motion through the new appropriate contact case subroutine.

In the next section, this method is used to calculate the final grasp configuration of the 3-DOF S-class finger described in section 2 as an example and the results are compared with the DSS.

5 Implementation and Results

Based on the previous analysis, a program has been developed and the Transmission matrix of a 3-DOF S-class finger has been established. To run the proposed method, design parameters of this finger are given as listed in Table 2. All the parameters in this table are defined according to Fig. 2 (the parameter a_2 has a negative value considering the positive direction shown in this figure). Furthermore, the stiffness coefficients of the springs located in the joints o_2 and o_3 are set to $0.01\ N.m/rad$. The coefficients w_i and h_i for $i = 1,2,3$ are respectively affecting the torques τ''_i and damping on the changes of the joint angles at each iteration. Depending on the contact case, their values in the corresponding subroutines are not the same. For these tests they are chosen to be $w_i \in [0.1,1]\ rad/(N.m)$ and $h_i \in [0.1,0.5]$.

The grasped objects are assumed to be defined by three contact points and are fixed with respect to the ground. The tests have been carried out with seven different triangular objects whose coordinates are shown in Table 3.

The result of the simulation of the closing motion of the finger during test no. 1 is shown in Figs. 5 and 6. As illustrated in Fig. 5, the algorithm first finds the initial configuration of the finger, where, the proximal phalanx is in contact with the object and the intermediate phalanx is on the verge of colliding with another vertex of the object. To find this configuration, it is assumed that before the first contact, the finger performs its closing motion slowly so that the dynamics effects on the joint angles are neglected (this is valid when the passive components are used in the structure of the finger, otherwise this assumption is not possible). Subsequently, the finger is assumed straight and the angles θ_2 and θ_3 are initially zero. After the first contact, since no reconfiguration can happen, computing the second contact between the other phalanges (here, it is the intermediate one) and the object is straightforward.

Following this initial step, the actuation torque is increased step-by-step and the corresponding set of joint angles is found. However, in this particular example the distal phalanx reaches its mechanical limit without colliding with the object and is stopped there. The increase of actuation torque is continued up to when the finger reaches a final configuration where, as mentioned before, increasing the value of actuation torque will not change its posture.

The evolution of the joint angles during this sequence is shown in Fig. 6. It can be seen in this figure that each time the actuation torque is increased, the current configuration becomes unstable and the finger is reconfigured with its angles moving toward a new set of values. In the graph of angle θ_3 in Fig. 6, the change of this angle due to the step-by-step increase of actuation force can be clearly observed.

This simulation has been tested with all the cases listed in Table 3 and the final sets of joint angles have been recorded. However, in some cases such as test no. 6, when the finger reaches its final configuration if the algorithm is not stopped and the value of the actuation torque is increased then, the configuration became unstable and the value of the joint angles oscillate. These oscillations are illustrated in Fig. 7. As it can be seen in this figure, after iteration no. 5941 these oscillations start and their amplitudes gradually increase.

Finally, this finger has been modeled with the DSS to compare the accuracy of the proposed method. To this aim, the

final values of the joint angles for all tests are again sought after. In Fig. 8, the final configuration of the finger found for the test no. 1 with the DSS is illustrated and in Fig. 9, the evolutions of the joint angles are shown. Comparing Figs. 6 and 9 reveals that the angles do not follow the same path to reach to the final configuration in these two methods which could have been expected. The reason for this is that in the proposed algorithm, the finger is assumed to reconfigure around local configurations with static equilibrium and as mentioned previously, the dynamic aspect of the process is neglected. Also, the algorithm evaluated the process iteratively so the x axes of Figs. 6 and 7 show the number of the iterations while the DSS software analyzed it dynamically so in Fig. 9 the x axis is in "sec".

Testing the closing motion of the finger with different dynamic properties (masses, inertias, etc.) in the DSS reveals that unless huge differences among the masses and inertias of the links exist, the final grasp configuration does not change for the same set of contact points (i.e., the same objects). This is because the final configuration of the finger depends on the location of the contact points, design parameters of the finger (i.e., links lengths) and also the values of the mechanical limits. Therefore, for the same initial contact configuration the ultimate sets of angles of the finger obtained with both methods are almost the same.

All final sets of angles found with both methods are listed in Table 4. As can be seen in this table, in most of the tests the differences between the angles found by both methods are less than 0.05° which demonstrates that the proposed method is accurate.

But, with a few tests the magnitude of the differences is larger. For instance, in test no. 6 the difference between the two final values of θ_3 is approximately 4.3°. In that case, considering the location of the contact points, small difference between the values of θ_2 between the two methods affects the corresponding position of axis o_3. Besides, if the distance between the third contact point and the axis o_3, k_3, is small then this difference is amplified. This issue results in a magnification of the difference between the values of θ_3. Besides, this algorithm is compared with a dynamic simulation package in which although the contact condition is modeled very close to what happens in the developed method but considering the realistic stiffness of the object and the phalanges and their very small penetration possibility in the DSS software and also their absolute rigidity in the algorithm, there are very short differences in the real positions of contact points (in the order of 0.01 *mm*). Therefore, part of these differences is also caused by this variance. However, the investigation on the results shows that this difference remains less than 1 degree for the proximal phalanx and less than 2 degrees for the intermediate phalanx. For the distal phalanx, if k_3 is at least 20 times bigger than the difference in the position of o_3 in two methods then the variance for angle θ_3 is less than 3 degrees, but if it is too small (i.e., $k_3 \to 0$) then it can be considerable and even be as large as the range of the angle θ_3.

However, although the method could not find an extremely accurate final configuration is some cases, it was able to approximate the final configuration of the finger in the right way. Improving the accuracy of this method for the entire workspace of the finger and generalizing its application to evaluate the grasp of un-fixed object by a multi finger system remains as the future work.

6 Conclusions

In this paper, a novel numerical method to evaluate the configuration of a 3-DOF underactuated finger and obtain its final grasp posture is introduced. This method calculates the signs and magnitudes of the torques which must be exerted to the finger through contact points to reach the final configuration. To illustrate this algorithm a S-class 3-DOF finger was chosen and analyzed. Afterwards, the behavior of this finger during the grasping of different objects with three fixed contact points has been tested and the results have been compared with a dynamic simulation software. The comparison of the results between the two methods showed that the proposed algorithm could properly analyze the reconfiguration of the finger and calculate its final posture.

References

[1] Kragten, G.A. and Herder, J.L., 2010, "The ability of underactuated hands to grasp and hold objects", Mech. Mach. Theory, **45**(3), pp. 408–425.

[2] Ceccarelli, M., Tavolieri, C., and Lu, Z., 2006, "Design considerations for underactuated grasp with a one D.O.F. anthropomorphic finger mechanism", Proceedings of the IEEE/RSJ International Conference on Intelligent Robots and Systems, Beijing, China, Oct. 9–15, pp. 1611–1616.

[3] Ciocarlie, M. and Allen, P., 2010, "Data-driven optimization for underactuated robotic hands", IEEE International Conference on Robotics and Automation, Anchorage, USA, May 3–7, pp. 1292–1299.

[4] Birglen, L., Laliberte, T., and Gosselin, C., 2008, *Underactuated Robotic Hands*, Springer-Verlag, New York, vol. 40.

[5] Krut, S., 2005, "A force-isotropic underactuated finger", Proceedings of the IEEE International Conference on Robotics and Automation, Barcelona, Spain, Apr. 18–22, pp. 2314–2319.

[6] Kragten, G.A., Kool, A.C., and Herder, J.L., 2009, "Ability to hold grasped objects by underactuated hands: performance prediction and experiments", Proceedings of the IEEE international conference on Robotics and Automation ,Kobe, Japan, May 12–17, pp. 3027–3032.

[7] LiCheng, W., Carbone, G., and Ceccarelli, M., 2009, "Designing an underactuated mechanism for a 1 active DOF finger operation", Mech. Mach. Theory, **44**(2), pp. 336–348.

[8] Ozawa, R., Hashirii, K., and Kobayashi, H., 2009, "Design and Control of Underactuated Tendon-Driven Mechanisms", Proceedings of the IEEE international conference on Robotics and Automation ,Kobe, Japan, May 12–17, pp. 287–292.

[9] Krut, S., Bgoc, V., Dombre, E., and Pierrot F., 2010, "Extension of the Form-Closure Property to Underactuated Hands", IEEE Trans. Rob., **26**(5), pp. 853–866.

[10] Steutel, P., Kragten, G.A., and Herder, J.L., 2010, "Design of an underactuated finger with a monolithic structure and largely distributed compliance", Proceedings of the ASME Design Engineering Technical Conference, Montreal, Canada, Aug. 15–18, pp. 355–363.

[11] Hirose, S. and Umetani, Y., 1978, "The development of soft gripper for the versatile robot hand", Mech. Mach. Theory,**13**(3), pp. 351–359.

[12] Crisman, J.D., Kanojia, C., and Zeid, I., 1996, "Graspar: A Flexible, Easily Controllable Robotic Hand", IEEE Robotics and Automation Magazine, pp. 32–38.

[13] Carrozza, M.C., Suppo, C., Sebastiani, F., Massa, B., Vecchi, F., Lazzarini, R., Cutkosky, M.R., and Dario, P., 2004, "The SPRING

Hand: Development of a Self-Adaptive Prosthesis for Restoring Natural Grasping", Auton. Robots, **16**(2), pp. 125–141.

[14] Kaneko, M., Higashimori, M., Takenaka, R., Namiki, A., and Ishikawa, M., 2003, "The 100 g capturing robot – too fast to see", IEEE/ASME Trans. Mechatronics, **8**(1), pp. 37–44.

[15] Massa, B., Roccella, S., Carrozza, M.C., and Dario, P., 2002, "Design and development of an underactuated prosthetic hand", Proceedings of the IEEE International Conference on Robotics and Automation, Washington, USA, May 11–15, pp. 3374–3379.

[16] Cabas, R., Cabas, L.M., and Balaguer, C., 2006, "Optimized design of the underactuated robotic hand", Proceedings of the IEEE international conference on Robotics and Automation, Orlando, USA, May 15–19, pp. 982–987.

[17] Yao, S., Ceccarelli, M., Carbone, G., and Lu, Z., 2009, "An Optimal Design for a New Underactuated Finger Mechanism", Proceedings of the IEEE/RSJ international conference on Intelligent robots and systems, St. Louis, USA, Oct. 11–15, pp. 2391–2396.

[18] Gosselin, C. and Laliberte, T., 1996, "Underactuated mechanical finger with return actuation", US Patent No. 5 762 390.

[19] Laliberte, T. and Gosselin, C. 2003, "Actuation System for Highly Underactuated Gripping Mechanism", US Patent No. 5 762 390.

[20] Luo, M., Carbone, G., Ceccarelli, M., and Zhao, X., 2010, "Analysis and design for changing finger posture in a robotic hand", Mech. Mach. Theory, **45**(6), pp. 828–843.

[21] Yang, D., Zhao, J., Gu, Y., Wang, X., Li, N., Jiang, L., Liu, H., Huang, H., and Zhao, D., 2009, "An Anthropomorphic Robot Hand Developed Based on Underactuated Mechanism and Controlled by EMG Signals", J. Bionic Eng. **6**(3), pp. 255–263.

[22] Kaneko, M. and Tanie, K., 1990, "Contact point detection for grasping of an unknown object using self-posture changeability (spc)", Proceedings of the IEEE International Conference on Robotics and Automation, Cincinnati, USA, May 13–18, pp. 864–869.

[23] Laliberte, T., Birglen, L., and Gosselin, C., 2002, "Underactuation in robotic grasping hands", Japanese Journal of Machine Intelligence and Robotic Control, Special Issue on Underactuated Robots, **4**(3), pp. 77–87.

[24] Ciocarlie, M. and Allen, P., 2009, "A design and analysis tool for underactuated compliant hands", IEEE-RSJ International Conference on Intelligent Robots and Systems, St. Louis, USA, Oct. 11–19, pp. 5234–5239.

[25] Song, P., Kraus, P., Kumar, V., and Dupont, P., 2001, "Analysis of rigid-body dynamic models for simulation of systems with frictional contacts", Trans. ASME, J. Appl. Mech., **68**(1), pp. 118–128.

[26] Birglen, L., 2009, "Type Synthesis of Linkage-Driven Self-Adaptive Fingers", ASME J. Mech. Rob., **1**(2), pp. 1–9.

[27] McCarthy, J.M., 2000, *Geometric design of linkages*, Springer-Verlag, New York, Vol. 11.

List of Table Captions

List of Figure Captions

Table 1. Contact cases between the phalanges and the object

Cases	Proximal phalanx	Intermediate phalanx	Distal phalanx
Case 1	√	√	√
Case 2	-	√	√
Case 3	√	-	√
Case 4	-	-	√
Case 5	√	√	-
Case 6	-	√	-
Case 7	√	-	-
Case 8	-	-	-

Table 2. Geometric parameters defining the analyzed finger (all dimensions are in mm)

a_1	a_2	L_1	L_2	L_3	b_1	b_2	c_3	ψ_3
0	-50	45	75	70	195	135	21	80°

Table 3. Coordinates of the vertices of the triangles with respect to the base frame of the finger (all positions are in mm)

Test No.	Point 1		Point 2		Point 3	
	X	Y	X	Y	X	Y
1	25	30	30	75	-20	90
2	-50	30	30	75	0	130
3	25	30	-50	75	0	160
4	-50	30	-50	75	0	130
5	25	30	30	75	0	130
6	25	30	-50	75	0	130
7	25	25	70	65	-100	80

Table 4. Final sets of joint angles obtained from both methods

		θ_1	θ_2	θ_3
Test No.1	Method	41.359	53.409	90.000
	DSS	41.423	53.309	90.011
Test No.2	Method	55.093	28.541	67.784
	DSS	54.647	29.479	66.900
Test No.3	Method	50.194	52.742	-0.004
	DSS	50.195	52.763	-0.051
Test No.4	Method	84.772	0.513	49.228
	DSS	84.779	0.435	49.523
Test No.5	Method	50.194	38.117	58.275
	DSS	50.195	38.116	58.303
Test No.6	Method	50.194	48.450	30.240
	DSS	50.194	49.889	25.920
Test No.7	Method	20.347	40.253	90.000
	DSS	20.332	40.320	90.040

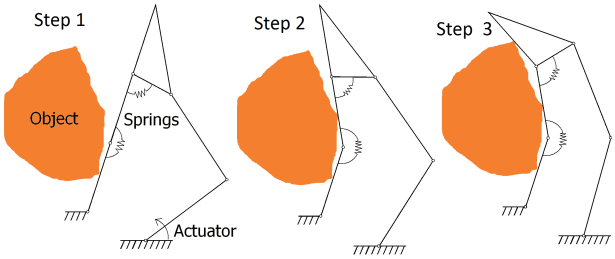

Fig. 1. Typical closing motion of an underactuated finger with three phalanges

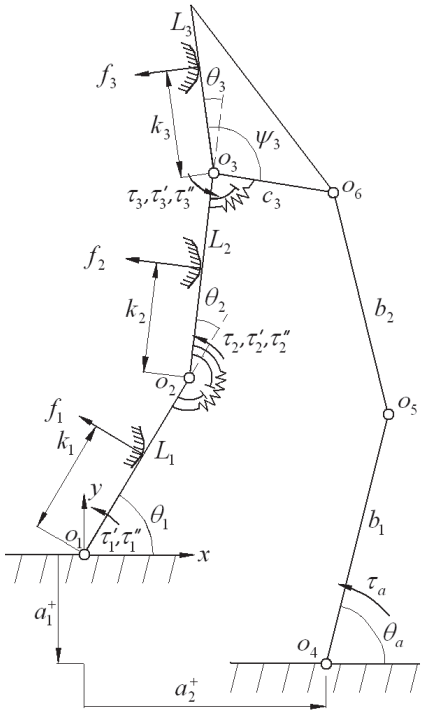

Fig. 2. Schematic of a 3-DOF S-class underactuated finger

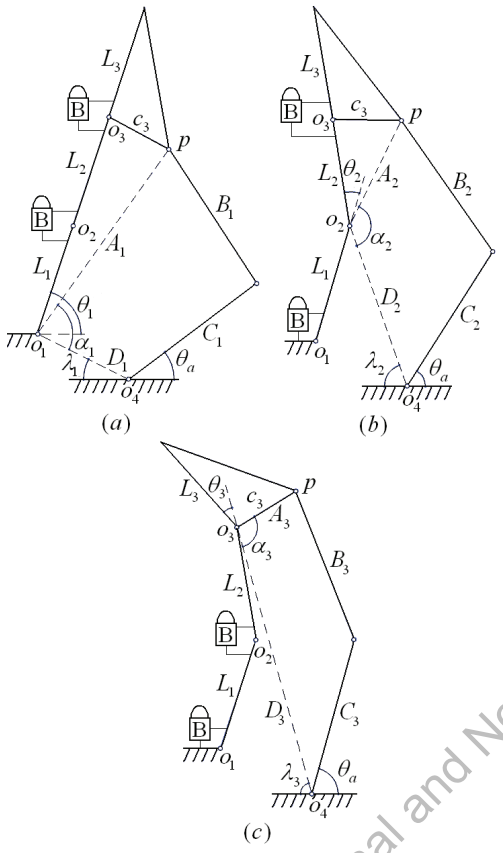

Fig. 3. Definition of the conceptual four-bar linkage during the closing motion of (a) the first joint, (b) the second joint, and (c) the third joint, the lock symbol indicates a non-rotating joint

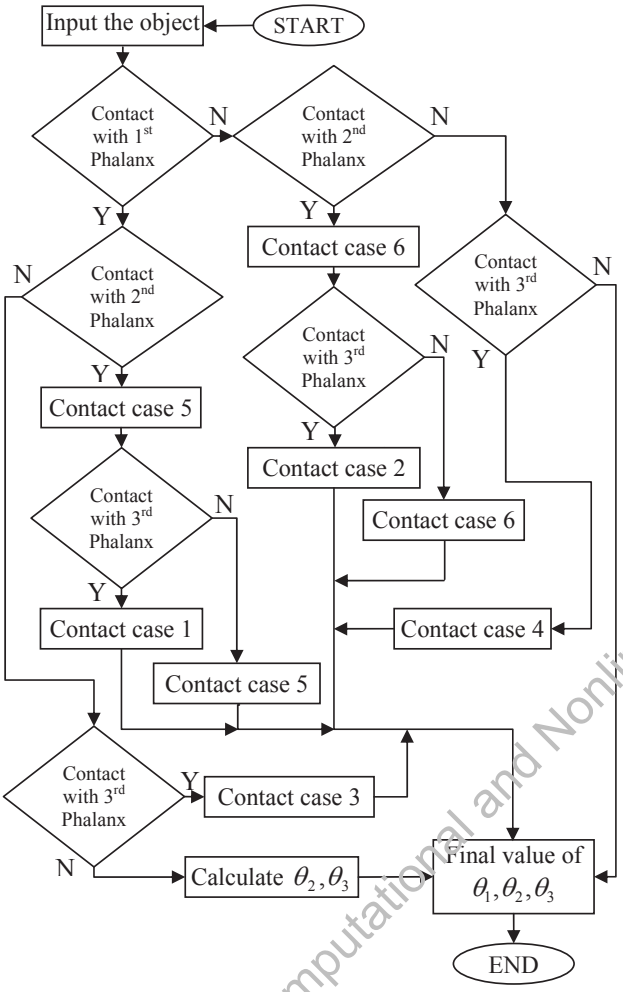

Fig. 4. Flow chart of the proposed numerical method

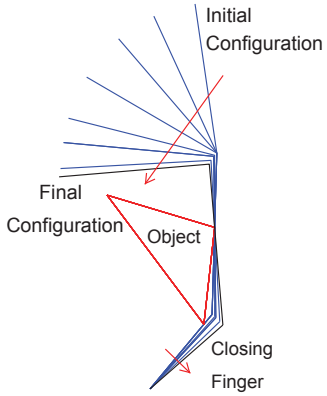

Fig. 5. Closing motion of the finger during test no. 1

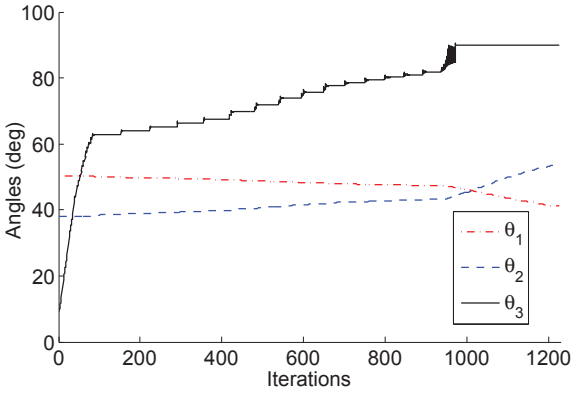

Fig. 6. Evolution of the joint angles during the closing motion of test no. 1

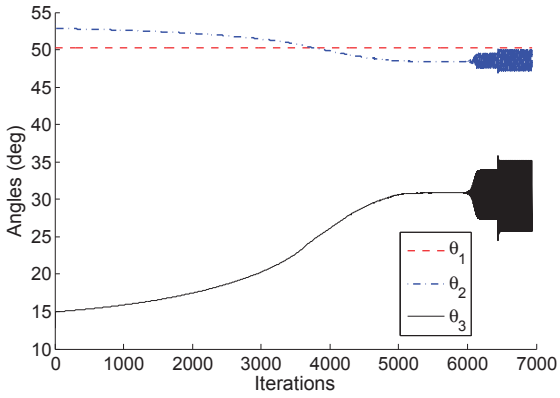

Fig. 7. Oscillations of joint angles after reaching the final configuration in test no. 6

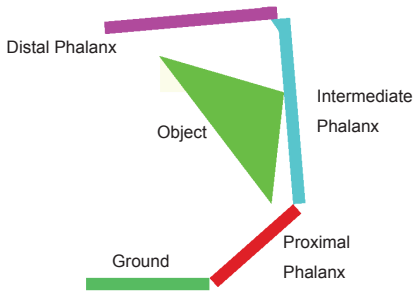

Fig. 8. Final configuration of the finger during test no. 1 with the DSS

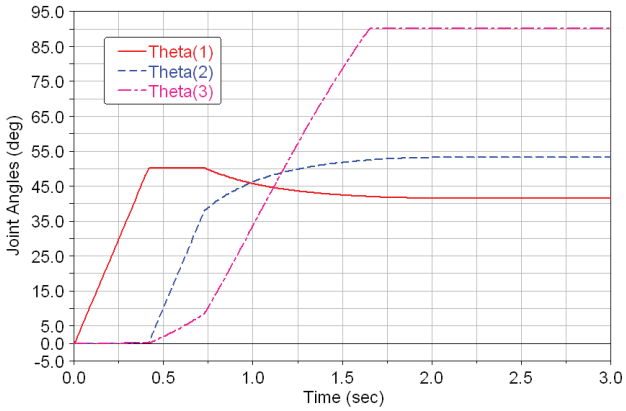

Fig. 9. Joint angles of the finger during test no. 1 with the DSS